Journal of Fluids and Structures (2001) **15,** 543–554
doi:10.1006/jfls.2000.0356, available online at http://www.idealibrary.com on IDEAL®

SPATIO-TEMPORAL RECONSTRUCTION OF VORTEX DYNAMICS IN AXISYMMETRIC WAKES

C. Brücker

Aerodynamisches Institut der RWTH Aachen
Wüllnerstr. zw. 5 u. 7, D-52062 Aachen, Germany

(Received 28 August 2000, and in final form 15 November 2000)

With time recording Digital-Particle-Image Velocimetry and spatio-temporal reconstruction technique, we obtained detailed quantitative results of the evolution of the velocity and vorticity field in the wake of axisymmetric bluff bodies—a sphere and an axially oriented cylinder with an elliptic nose and a blunt base. Experiments were carried out for Reynolds numbers of Re = 500, 700 and 1000 in the transition range from "regular" to "irregular" shedding. DPIV-recordings in radial cross-sections at several distances downstream of the bodies allowed us to reconstruct the dynamics of the streamwise vorticity over a large number of shedding cycles. Our results prove that the wake in this regime consists of a double-sided chain of oppositely oriented hairpin vortices. In addition, the results show a well-defined low-frequency modulation of the vortex shedding, with a distinct peak in the frequency spectrum at a Strouhal number of about Sr $\approx$ 0·05 (in case of the sphere). The wake pattern in this "irregular" shedding regime typically exhibits periodic packets of 3–4 "regular" shedding cycles which are interrupted by phases with less action. The results indicate the coexistence of a long-wave instability of axisymmetric wakes against helical waves in addition to the primary instability causing the vortex shedding process.

1. INTRODUCTION

The present study was undertaken with the objective of a detailed quantitative analysis of the evolution of the flow field in the wake of axisymmetric bluff bodies like spheres and spheroids. While much experimental data exist for the wake of nominally two-dimensional bodies like the cylinder wake, considerably less has been reported on wake flows of axisymmetric bodies, although there is certainly the same strong physical and technical interest. Practical examples are the wake behind bubbles, drops and particles or projectiles and rockets. In comparison to the cylinder wake, the wake of axisymmetric bodies—from which the sphere wake is the most prominent—exhibits grave differences in the shape and dynamics of the vortices being shed. The wake structures are basically three dimensional and highly unsteady, which makes any measurements and interpretations difficult. To the best of the author's knowledge, any experiments which could provide detailed instantaneous flow field data in such type of wakes are still lacking. In addition, it is only recently that the progressively growing computing power has enabled the first numerical simulations of the unsteady wake flow of axisymmetric bodies (Johnson & Patel 1999; Mittal 1999; Lee 2000). Therefore, most of today's knowledge about the vortical structures contained in the wake is still based mainly on earlier flow visualisation studies (Magarvay & Bishop 1961; Achenbach 1974; Nakamura 1976; Sakamoto & Haniu 1990). For the sphere wake, these experiments revealed several stages in the transition of the wake from a steady axisymmetric wake to unsteady irregular vortex shedding. Up to Reynolds numbers of 130, the wake is stationary and forms an axisymmetric recirculating eddy. Beyond that, a weak

0889–9746/01/040543 + 12 $35.00/0

periodic wave-like wake with a long period was observed behind the axisymmetric eddy. In the range $210 < \mathrm{Re} < 270$, the wake evolves into an attached hairpin-like vortex, with its legs forming a pair of streamwise vortex filaments pointing downstream. As this wake pattern appears, the wake still seems to be stationary as reported by Nakamura (1976). For higher Reynolds numbers, up to $\mathrm{Re} = 420$, the flow visualisation experiments revealed a shedding of hairpin-like vortex structures. The wake appears as a chain of hairpin vortices with the heads pointing always to the same side in the same axial plane (Achenbach 1974). This pattern becomes irregular at increased Reynolds numbers.

Recent numerical simulations of the sphere wake flow by Johnson & Patel (1999) demonstrated that most of the flow visualisation experiments have overlooked vortex structures in the wake which are induced within the fluid and are not connected with the base of the bluff body. These occur as oppositely oriented hairpin vortices in-between the one-sided chain of hairpin vortices seen in the flow pictures from Nakamura (1976) and other authors. This discrepancy highlights that detailed chronological flow field measurements are necessary in order to provide the velocity and vorticity information for the entire wake. The objective of the present paper is to fill this gap in experimental knowledge by detailed analysis of the structure and dynamics of the vortices in the wake. Therefore, we applied chronological high-speed DPIV-technique to capture the temporal evolution of the flow field in radial cross-sections downstream of the axisymmetric bluff bodies. The time-series of DPIV results are used to analyze the vortex dynamics with the aid of spatio-temporal reconstruction method. The most relevant studies with respect to our work are the numerical simulations done by Tomboulides & Orszag (2000), Mittal (1999), Johnson & Patel (1999) and, most recently, the work from Lee (2000) which was published during the completion of this article. Of particular interest in Lee's paper is his observation of a low-frequency fluctuation, in addition to the primary vortex shedding which is one particular focus of our work.

2. EXPERIMENTAL METHODS AND ARRANGEMENT

The test-objects chosen in our study were a solid sphere and a cylindrical rod with an elliptical nose and a sharp trailing edge (Figure 1) which is aligned with its axis along the flow axis. In contrast to the sphere, the cylinder has a defined separation edge and the boundary layer thickness can be controlled by the length. This allows us to study the effect of boundary layer thickness on the stability of the wake. The experiments were carried out in a vertical water channel shown in Figure 1. The transparent test-section has a cross-section of $10 \times 10\ \mathrm{cm}^2$ and is 1·2 m high. The bluff bodies with a diameter of 3 cm were held by a thin hollow rod of 2 mm diameter in the centre of the channel. To reduce its effect on the flow around the body, we sucked the boundary layer fluid away through tiny holes along the rod. Small tracer particles (Vestosint, mean diameter of 30 μm, $\rho = 1{\cdot}02\ \mathrm{g/cm}^3$) were added to the fluid upstream in the water basin and were mixed homogeneously.

The DPIV set-up was arranged to measure the velocity field in a horizontal cross-section, downstream of the body in order to obtain the distribution of streamwise vorticity in that plane. The beam of a continuous Ar^+ laser was expanded with a rotating polygonal mirror to form an intense virtual light-sheet in a horizontal cross-section of the channel. A digital high-speed video camera (resolution: 512×512 pixels; frame rate: 1000 Hz) was used to record the flow, synchronized with the polygonal mirror so that each frame corresponds to a single sweep of the laser beam. The recording rate was increased with the Reynolds number of the flow beginning from 60 Hz at $\mathrm{Re} = 300$, 100 Hz at $\mathrm{Re} = 500$, 200 Hz at $\mathrm{Re} = 700$ and 500 Hz at $\mathrm{Re} = 1000$. Within the horizontal light-sheet plane (y–z plane), the in-plane velocity components were obtained from cross-correlation of successive image

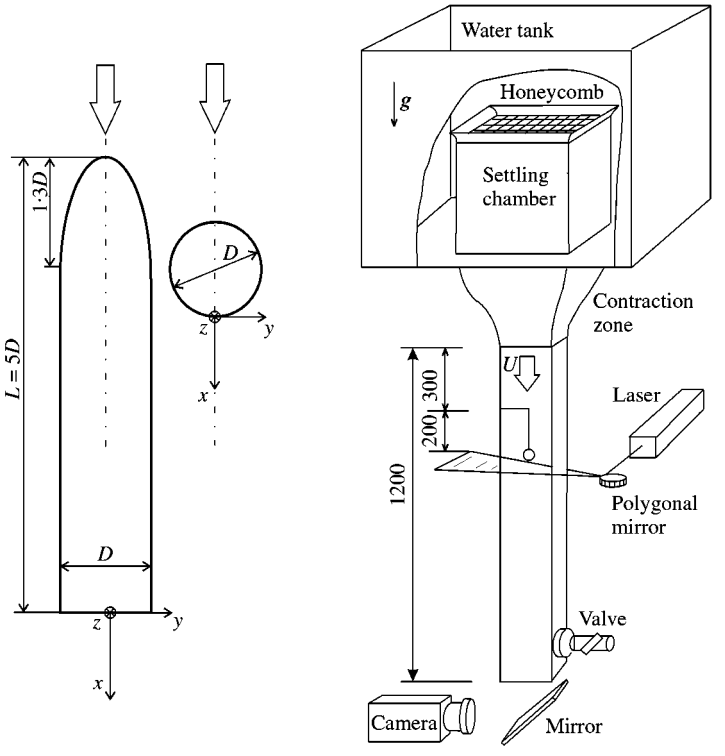

Figure 1. Experimental set-up and shape of the two axisymmetric bluff bodies used in this study.

pairs in small interrogation windows. The results represent a two-dimensional data set, in the form of velocity vectors on a grid with 31×31 equidistant nodes over a square cross-section area of $5 \times 5\ \mathrm{cm}^2$. The streamwise vorticity component was determined out of the velocity field by calculating the gradients in the 3×3 neighbourhood of each node using central difference schemes.

In all experiments, the measurement plane was located at $x = 3$ diameters downstream of the body base plane. At this position outside of the attached part of the wake, the vortex structures have not yet deformed by self-induction and are still mainly oriented in the streamwise direction while they are convected downstream; cf. the results from Tomboulides & Orszag (2000), Johnson & Patel (1999) and Mittal (1999). This enables to reconstruct the dominant part of the vortex structures by spatio-temporal display of the chronological DPIV results in the radial cross-sections.

3. RESULTS

Before we discuss the results by means of the spatio-temporal reconstruction images, an example of the dynamics of the bluff-body wake is first shown in a sequence of DPIV results in the following section.

3.1. Sphere Wake at $\mathrm{Re} = 400$

Figure 2 gives an example of the instantaneous flow field in the radial cross-section at $x = 3$ diameters downstream of the sphere for a Reynolds number of 400. The flow field shows

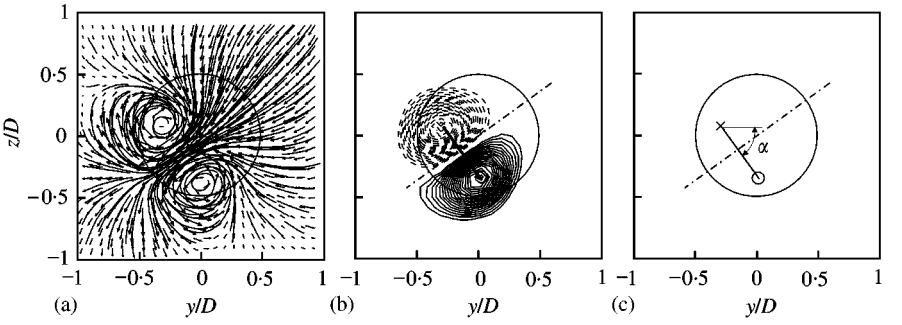

Figure 2. Example of DPIV results in the wake of a sphere (Re = 400) in a cross-section at $x/D = 3$: (a) velocity field and sectional streamlines, integrated from the velocity field; (b) lines of constant streamwise vorticity with constant increment (continuous lines indicate positive rotation, dashed lines indicate negative rotation). (c) Definition of the angular orientation of the wake.

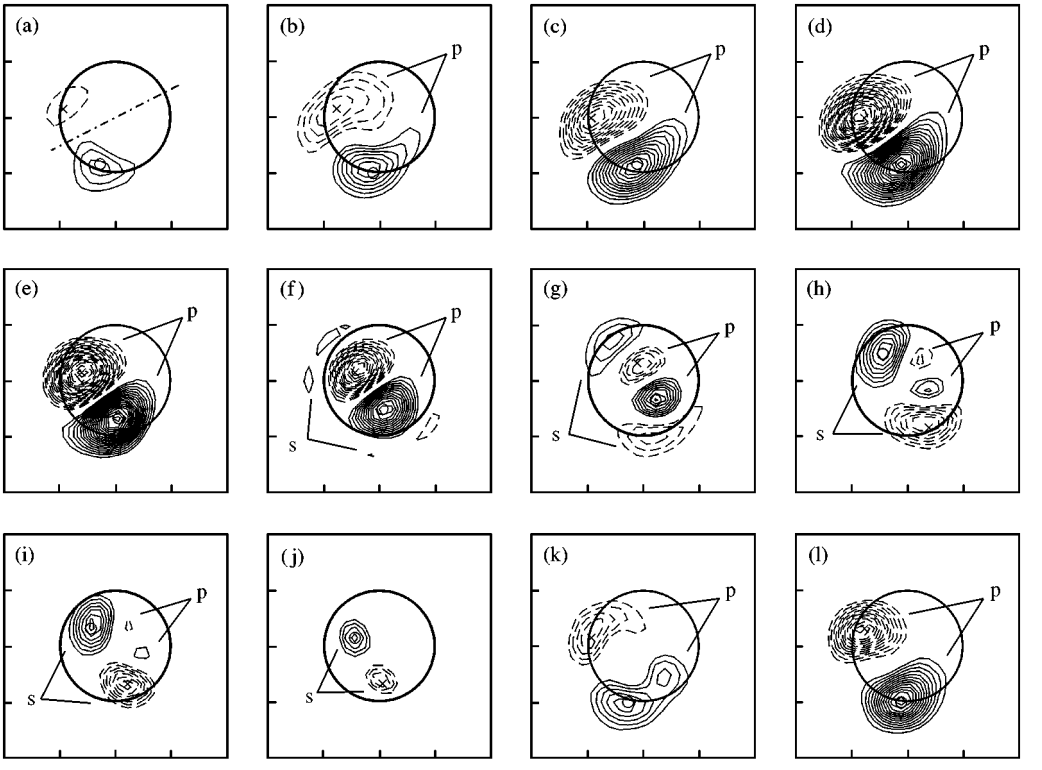

Figure 3. Evolution of the streamwise vorticity distribution in the wake of a sphere (Re = 400) in a cross-section at $x/D = 3$ over a complete shedding cycle; the mark "p" indicates the primary vortex pair, "s" the secondary pair.

a pair of streamwise vortices in the cross-section of the wake, which represent cuts through the legs of the vortex loop being shed into the wake. Note that the vortex pair is not located at the centre of the sphere-wake but offset to the lower left side. A strong radial cross-flow is induced between the vortices. The induced flow field exhibits a symmetry of the wake about a plane passing through the wake centreline, tilted about an angle of 45°; the vortex centres

of the pair are mirror-symmetric to this plane. The orientation of the vortex pair (which is referred to as the "wake orientation") is defined by the angle α of the connection line between the vortex centres, which we determine from the extrema of streamwise vorticity in our data. The temporal signal of this angle is used to display the angular stability of wake orientation in different stages of wake transition. In addition, the average value of positive streamwise vorticity and its variation over time is used as a first approximation of the variation of the strength of the vortices. An additional value of interest is the radial velocity component at the centreline.

The dynamics of the wake is shown in Figure 3 by a sequence of DPIV results over one single shedding cycle. During the cycle, the vortex pair (a "pair" is characterized by two regions with concentrated streamwise vorticity of opposite sign which are symmetrically positioned at opposite sides of the plane of symmetry) varies in strength and size and moves along the plane of symmetry. Both parts of the pair remain in their same angular relation and strength relative to each other, over the entire shedding cycle. Therefore, the angular orientation is maintained at a fixed plane of symmetry at all times during the shedding process, which is an intrinsic feature of the sphere wake at this range of Reynolds numbers. From Figure 3(a) to 3(d) the primary vortex pair, which is offset outside the centreline to one side of the sphere, grows in strength and size. Then the vortex pair starts to move towards the centreline, loses its strength, shrinks (both centres approach each other), until it has finally diminished in Figure 3(i). Meanwhile, one can see the generation of a secondary vorticity pair at the outer shoulders of the primary vortex pair with counter sign of rotation [Figures 3(f,g)]. This secondary pair shows the same trend over time as the primary pair, as it grows in strength [Figures 3(g,h)], starts to move towards the centre of the wake [Figures 3(h,i)], shrinks again and finally diminishes [Figures 3(j,k)]. Now the cycle is finished and the next one starts at Figure 3(k) with the appearance of a new primary vortex pair at the left side of the sphere, similar as in Figures 3(a,b).

The contours of regions of concentrated streamwise vorticity of the secondary vortex pair displayed in Figure 3 show that this pair never reaches the same size and strength compared to that of the primary pair. This, together with the observation that the secondary pair is generated at the outer shoulders of the primary vortex pair, suggests that the vorticity of the secondary pair is not being shed from the sphere but results from the roll-up of the shear layer between the outer flow and the strong swirling flow around the vortex tails of the primary vortex pair. Comparing our data with the results from Johnson & Patel (1999) let us conclude that the secondary pair reflects an induced hairpin vortex, while the primary pair reflects a shed hairpin vortex. The induced vortex structures—as they describe—are generated by the interaction of the near wake flow and the outer flow and are based on a different mechanism as the shed hairpin. Unfortunately, the limited information given in their paper does not allow a direct comparison of the streamwise vorticity distribution. Nevertheless, one can see from figure 29 in their article that the streamwise vorticity within the shed hairpin vortices is higher than in the induced hairpin vortices which agrees with our observation, too. Note also that the primary vortex pairs always evolves on the same side of the sphere, which means that the vortices shed only from one side in our experiments, as in the numerical results.

The spatio-temporal reconstruction of the vorticity field is in principle created from a time sequence as given in Figure 3, using the complete data set with a much higher temporal resolution and a total recording period of over several tens of shedding cycles. The vorticity values in the horizontal plane were taken from the results and stacked plane by plane vertically in a data cube over the complete sequence of DPIV results in the recorded period. The resulting data matrix can be displayed as an isosurface of constant streamwise vorticity which gives an image of the spatio-temporal evolution of the component of

streamwise vorticity at a stationary location within the wake. The following figures display the resulting images of the isosurfaces of streamwise vorticity from two orthogonal viewing sides (front view and side view, which allow recognition of the orientation of the vortex structures in the plane of symmetry) together with the temporal evolution of the radial velocity at the centreline, the phase angle θ, the average value of positive axial vorticity and its power spectrum. The time unit is made dimensionless with the free-stream velocity and the diameter of the body.

3.2. Cylinder Wake and Sphere Wake at Re = 500

Figures 4 and 5 show the results for the cylinder and the sphere wake at a Reynolds number of 500. Note, that the isosurfaces are rotated such that the front view is along the plane of symmetry. The isosurfaces illustrate the periodic alternate downwash of oppositely oriented vortex pairs in the wake of the bodies over a period of about 14–15 cycles taking 80 time units. A comparison of the wake of the sphere (Figure 5) with the wake of the cylinder (Figure 4) shows that the boundary layer thickness has a strong influence on the stability and coherence of the vortex shedding. The sphere wake exhibits already the typical slight random variations of the orientation of the vortices and some "irregularity" in the shedding cycle. In comparison, the wake of the cylinder is approximately perfect periodic in time, with a stable orientation of the vortices (compare the phase angle plot in Figure 4). The strong coherence of the cycles in Figure 4 demonstrates the near periodic creation and discharge of the vortices which is similarly observed for the sphere wake at Reynolds numbers of less than about 420.

A typical pattern of a single cycle appears in the front view as a vertically stretched lambda-like vortex pair (the primary vortex pair marked "p") with a second shorter vortex pair (the secondary vortex pair marked "s") lying on top on its shoulders. Such a pattern would come out from spatio-temporal reconstruction of the cycle shown in Figure 3. The radial distance of the vortices of the primary pair decreases from bottom to top, giving the lambda-like shape. This corresponds—in the temporal evolution—to the convergence and shrinking of the vortex pair shown in Figures 3(d–h). As already concluded above from comparison of our results with the figures published by Johnson & Patel (1999) the vortex pairs represent parts of the actual three-dimensional hairpin-like vortices, namely the streamwise oriented legs.

Overall, our results clearly confirm a one-sided chain of the primary vortices in the wake which are interconnected with counter-oriented vortices of seemingly lower strength. The side views of the isosurfaces show that the induced hairpin vortices always point to the opposite side of the shed hairpin vortices and are of shorter vertical extension than the shed hairpin vortices. This is also well displayed in the evolution of the phase angle which we determined from the orientation of the dominant vortex pair. The moments at which the phase angle jumps about a value of π characterize the change of the dominant vortex pair in the cross-section from the shed hairpin vortex to the induced one and *vice versa*. The period in which the primary vortex pair dominates the flow in one cycle is considerably longer in the diagram of the phase angle than the period in which the secondary pair occurs. In addition, the evolution of the average value of positive streamwise vorticity—chosen as a first approximation to estimate the circulation of the hairpin-like vortices—shows that the vorticity in the phase of a primary vortex pair exceed that in the phase of a secondary vortex pair about a factor of 3–4 which indicates a low circulation of the induced hairpin vortices compared to the shed vortices.

An interesting feature can be deduced from the variation of the strength of the vortices over time (or the variation of the radial velocity at the centreline) in Figure 4. There is

a slight low-frequency modulation of the overall strength of the vortices which appears as a small peak in the spectrum at Sr = 0·015, in addition to the dominant peak at Sr = 0·168 representing the "natural" vortex shedding. The effect of this modulation is however so small that it does not change the overall pattern of vortex dynamics. In the sphere wake, we can see a similar low-frequency modulation of the strength of the vortices (Figure 5). It can be recognized in the evolution of the vorticity and its power-spectrum but also in the spatio-temporal reconstruction image. The plot of streamwise vorticity clearly displays a sinusoidal low-frequency modulation of the strength of the vortices which show peak vorticity values at $t \approx 10$, 30, 50 and 70. The power spectrum shows a peak at a Strouhal-number of Sr = 0·05 corresponding to this modulation. The second peak at Sr = 0·178 belongs to the vortex shedding and falls well within the range of values reported by Sakamoto & Haniu (1990) and Tomboulides & Orszag (2000).

The variation of the strength of the vortices leads to a variation of the shedding period and the inclination angle of the loops against the vertical. The inclination of the vortex pair is strictly coupled to the strength of the vortices since it is a result of the self-induction effect which scales with the circulation of the loops. It is well seen in the isosurfaces that in phases of high circulation of the loops, the vertical distances between successive vortex loops are shorter and the loops are more inclined against the vertical. In phases of less vorticity action the induced hairpin vortices reduce in size and strength in the same way as the shed hairpin vortices and sometimes even disappear. The mark "A" in Figure 5 indicates an interval $40 < t < 45$ where shedding is completely suppressed. The isosurface displays a temporarily stable vortex pair, similar as it is observed in form of the "double-threaded" wake at Re < 290. As a result of the variation of the shedding period the power spectrum reveals a double-peak scenario; the peak at Sr = 0·225 corresponds to the typical shedding period at high vorticity action around the times $t \approx 10$, 30, 50 and 70, while the peak at Sr = 0·178 corresponds to the "natural" shedding phases in between.

3.3. Cylinder Wake and Sphere Wake at Re = 700

For the cylinder wake, the discovered low-frequency instability of the wake and the resulting effect on the vortex structures becomes dominant at Re = 700, shown in Figure 6. The vortices seem to be shed in "pockets" of 3–4 strong hairpin vortices, interrupted by shedding phases with weaker hairpin vortices. The strong phases are marked as "A", "B" and "C" in Figure 6. The beginning of such a phase is coupled with a steep increase of the vorticity of the first hairpin and a flat decrease of the peak values for the following shedding cycles. The temporal profile of the mean vorticity shows a sawtooth-like envelope. The strength and size of the induced hairpin vortices are strictly coupled to that of the shed hairpin vortices, i.e., when the shed hairpin vortex is of higher circulation then it induces a stronger hairpin and vice versa. Similar to the sphere wake one can observe a faster shedding in phases of higher vorticity and a higher inclination of the loops to the vertical. The sawtooth-like envelope of variation of vorticity and the varying shedding frequency indicate a non-linear interaction of the low-frequency modulation and the "natural" shedding process.

The power-spectrum reveals—similarly as for the sphere—a double-peak scenario corresponding to the different phases of the shedding; the peak at Sr = 0·192 corresponds to the typical shedding period with high vorticity action around the times $t \approx 20$, 50, 80 in Figure 6, while the peak at Sr = 0·154 corresponds to the "natural" shedding phases in-between. One additional important aspect of the results in Figure 6 is that the angular orientation of the wake seemingly remains stable (except for a very small rotational drift of the entire wake in one direction, which results in a total rotation of 30° over the complete process with 100

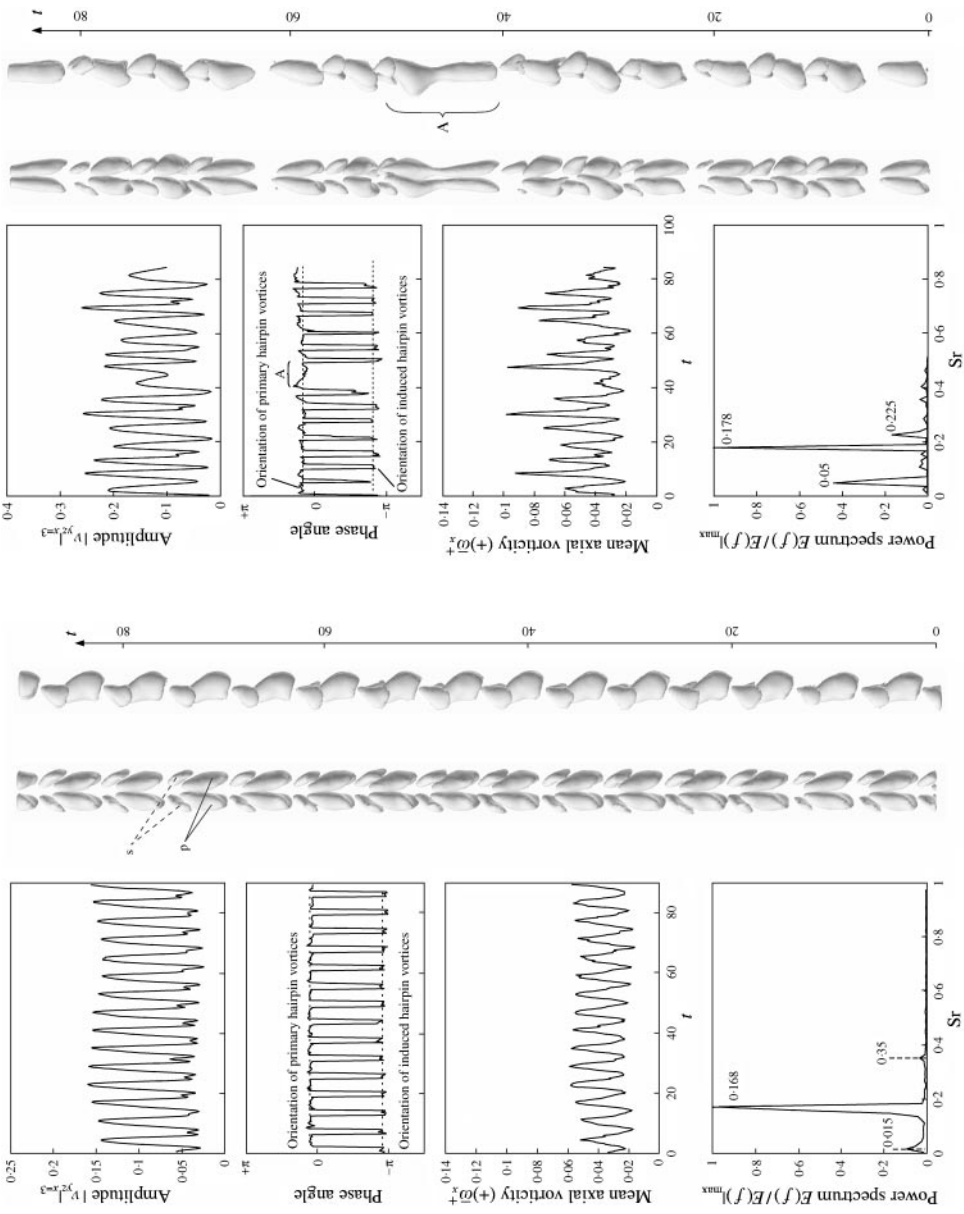

Figure 5

Figure 4

Figure 4. Dynamics of streamwise vorticity in the wake of the cylinder at Re = 500. The spatio-temporal behaviour of the streamwise vorticity component in the plane $x/D = 3$ is illustrated as isosurfaces of positive and negative vorticity in front and side view. On the left-hand side from the top to the bottom are plotted for different quantities in the plane $x/D = 3$ over the normalized time t: plot of the radial velocity at the centreline; plot of the phase angle; plot of the mean streamwise vorticity; power spectrum of the streamwise vorticity.

Figure 5. Same as Figure 4, but for the wake of the sphere at Re = 500.

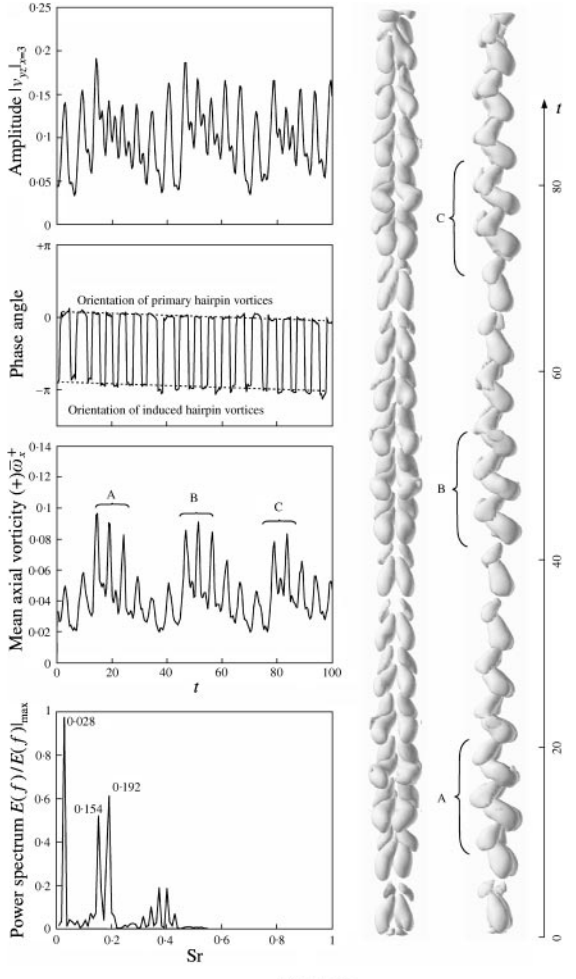

Figure 6

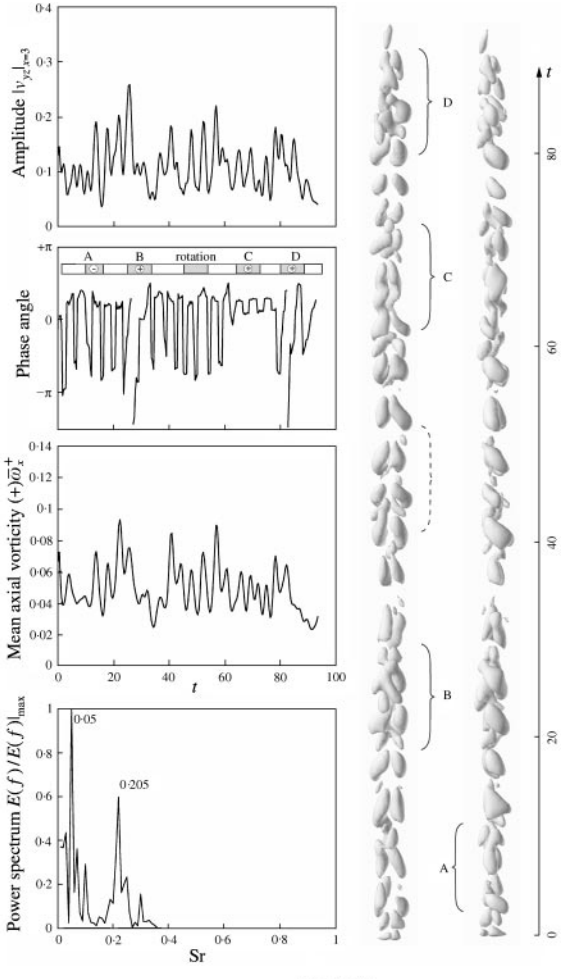

Figure 7

Figure 6. Same as Figure 4, but for the wake of the cylinder at Re = 700.

Figure 7. Same as Figure 4, but for the wake of the sphere at Re = 700.

time-units). The existence of the low-frequency fluctuation is therefore seemingly not necessarily coupled to a rotation of the detachment point of the vortex loop from the base of the body as speculated by Lee (2000). Rather, our results indicate that the low-frequency modulation is a generic instability of axisymmetric wakes to long-wavelength waves from which the helical-type waves are the most likely, according to the instability analysis by Natarjan & Acrivos (1993).

Figure 7 shows the results for the sphere wake at Re = 700. In comparison to the cylinder wake, the planar symmetry seems already to be lost and a more irregular pattern of vortex shedding is seen. The power spectrum of the vorticity shows the dominant peak at Sr = 0·05 which proofs that the low-frequency modulation is still present. The second peak at Sr = 0·205 corresponds to the vortex shedding. One can best see, similarly to the cylinder wake, the low-frequency modulation from the vorticity and velocity profile. In phases with a more stable orientation of the wake, as for example in the period $40 < t < 60$, the isosurfaces show a similar pattern as in the cylinder wake at Re = 700. Between the stable phases one can observe a twisting or rotation of the whole wake structure, which we have marked with "A–D" in Figure 7. These phases seem to be coupled with a steep increase of the vorticity; the vorticity peak at $t = 22$ initiates phase B, the peak at $t = 58$ initiates phase C and the peak at $t = 78$ initiates phase D. The peak at $t = 40$ is the only one which does not immediately lead to a twisting of the wake. It lets us conclude that the sphere wake at higher Reynolds numbers reacts to the long-wavelength modulation with a rotation or twisting of the wake, unlike the cylinder wake which still remains stable at Re = 700. Note, that the vortex loops themselves are also twisted in phases A, B and D, which means that the rotation continues over the shedding process, sometimes even over periods of 2–3 cycles.

The power spectrum of the vorticity signal does not show anymore the typical double-peak scenario in the shedding regime but only a broader single peak at Sr = 0·205. However, one can still see a variation of the shedding frequency in the profile of the phase angle comparing the times at which the phase angle jumps about π. We believe that possibly the vorticity signal—especially during the wake rotation—does not reflect anymore a proper value to identify the shedding frequency; this might be the reason that an actual double-peak scenario has converged to a single broader peak in the power spectrum. A similar transition of the overall pattern as observed herein for the sphere at Re = 700 is also observed for the cylinder wake at a higher Reynolds number of Re = 1000, for which results cannot be shown here due to space limits.

4. DISCUSSION AND CONCLUSION

In general, the wake transition process shows similar patterns for the cylinder and the sphere wake, except the fact that, for the cylinder wake, the transition is shifted to higher Reynolds numbers. The planar symmetry of the sphere wake at Re = 400 is lost at Re = 500 in our experiments. For the cylinder wake this regime extends to at least Re = 500. First, slight fluctuations of the phase angle occur at Re = 700, which is comparable to the sphere wake at about Re = 500. This suggests that the boundary-layer thickness plays an additional role in the instability of axisymmetric wakes in the way that an increased boundary layer thickness seemingly stabilizes the wake orientation. DPIV measurements in the cross-section downstream of the sphere and the cylinder show that the overall shape of the generated vortices resembles hairpin-like structures. The legs are represented by the measured centres of streamwise vorticity in the cross-section. The reconstructed isosurfaces display a chain of hairpin vortices which consists of an alternate arrangement of a shed hairpin vortex followed by an induced, oppositely oriented hairpin vortex. A similar result is

documented in recent numerical results of sphere wake flow at $\mathrm{Re} = 300$ by Johnson & Patel (1999). A lower strength of the induced hairpins is observed here, too.

A possible explanation of the planar symmetry and its loss at higher Reynolds numbers will be discussed in the following from the interaction of helical waves in axisymmetric wakes. Natarajan & Acrivos (1993) found, via a global stability analysis, that axisymmetric wake flows are most unstable against helical waves. The first instability in the sphere wake appears for a nonfluctuating helical wave with an azimuthal wavenumber of $k = 1$ (this means that the wavelength fits once within the circumference), i.e., the wake becomes asymmetric but remains steady. Beyond this first critical Reynolds number, the flow becomes unstable to fluctuating helical waves with $k = 1$, and the flow becomes unsteady. It is obvious from the planar symmetry of the wake in the range $290 < \mathrm{Re} < 420$ that two counter-rotating helical waves must exist simultaneously, which additionally must have the same amplitude and phase velocity. If so, the counter-rotating waves leads to a perfect planar oscillations of the wake which can be proved by simple additive superposition of both waves. However, if this system is destabilized, one of these helical waves would dominate, which would lead to a helical deformation of the wake. Our results suggest that this is what happens for higher Reynolds numbers, in which those phases with wake rotation are initiated by the low-frequency modulation of the wake as discussed in what follows.

Most interestingly in our experiments, we could identify a previously overlooked low-frequency modulation of the wake; the vortex patterns show a long-wavelength periodic variation of the circulation and shedding frequency of the hairpin vortices. The hairpin vortices with a higher circulation appear periodically in packets of 3–4 vortices which are more inclined against the vertical and shed more rapid in comparison to the phases of "natural" vortex shedding at frequencies which agree with those reported in earlier studies [see, e.g., Sakamoto & Haniu (1990)]. As a result, the shedding regime appears in the power spectrum of the vorticity signal as a double-peak scenario. In addition, a third peak indicates the low-frequency modulation at a Strouhal number of $\mathrm{Sr} = 0{\cdot}05$ in the sphere wake and $\mathrm{Sr} = 0{\cdot}03$ in the cylinder wake. It is assumed that the low-frequency modulation is again linked to helical-type waves with an azimuthal wave-number of $k = 1$ according to the results from Natarajan & Acrivos (1993). This demonstrates that there is an interaction of instabilities at different characteristic frequencies which was not observed in experiments before.

While this low-frequency modulation seems to destabilize the planar symmetry of the sphere wake at $\mathrm{Re} = 500$, it does not have a significant effect on the planar symmetry in the wake of the cylinder up to $\mathrm{Re} = 700$. This suggests that the long-wave instability appears again as a pair of counter-rotating helical waves of the same amplitude and phase velocity. This instability exists over the entire transition range of the cylinder flow with a Strouhal number of $\mathrm{Sr} = 0{\cdot}015$ at $\mathrm{Re} = 500$, $\mathrm{Sr} = 0{\cdot}028$ at $\mathrm{Re} = 700$, and $\mathrm{Sr} = 0{\cdot}03$ at $\mathrm{Re} = 1000$. At the higher Reynolds number, both the cylinder and the sphere wake show that the symmetry is not completely lost but reappears periodically in phases with regular shedding and a seemingly stable orientation, over 3–4 shedding cycles. This lets us conclude that the loss of planar symmetry in axisymmetric wakes is the primary consequence of the imbalance of the long-wave helical waves.

ACKNOWLEDGEMENTS

The author wishes to acknowledge support from the Deutsche Forschungsgemeinschaft DFG through the Habilitationsstipendium Br 1494 /2-1

References

ACHENBACH, E. 1974 Vortex shedding from spheres. *Journal of Fluid Mechanics* **62,** 209–221.

JOHNSON, T. A. & PATEL, V. C. 1999 Flow past a sphere up to a Reynolds Number of 300. *Journal of Fluid Mechanics* **378,** 19–70.

LEE, S. 2000 A numerical study of the unsteady wake behind a sphere in uniform flow at moderate Reynolds-number. *Computers and Fluids* (to appear).

MAGARVAY, R. H. & BISHOP, R. L. 1961 Transition ranges for three-dimensional wakes. *Canadian Journal of Physics* **39,** 1418–1422.

MITTAL, R. 1999 Planar symmetry in the unsteady wake of a sphere. *AIAA Journal* **37,** 388–390.

NAKAMURA, I. 1976 Steady wake behind a sphere. *Physics of Fluids* **19,** 5–8.

NATARAJAN, R. & ACRIVOS, A. 1993 The instability of the steady flow past spheres and disks. *Journal of Fluid Mechanics* **254,** 323–344.

SAKAMOTO, H. & HANIU, H. 1990 A study of vortex shedding from spheres in a uniform flow. *ASME Journal of Fluids Engineering* **112,** 386–392.

TOMBOULIDES, A. G. & ORSZAG, S. A. 2000 Numerical investigation of transitional and weak turbulent flow past a sphere. *Journal of Fluid Mechanics* **416,** 45–73.